Properties of quenched $LiFePO_4$/C powder obtained via cellulose matrix-assisted method

Dragana Jugović[a], Miodrag Mitrić[b], Miloš Milović[a], Bojan Jokić[c], Marija Vukomanović[d], Danilo Suvorov[d], Dragan Uskoković[a]

[a]Institute of Technical Sciences of SASA, Knez Mihailova 35/IV, 11 000 Belgrade, Serbia

[b]Vinča Institute of Nuclear Sciences, University of Belgrade, P.O. Box 522, 11 001 Belgrade, Serbia

[c]Faculty of Technology and Metallurgy, University of Belgrade, Karnegijeva 4, 11 000 Belgrade, Serbia

[d]Advanced Materials Department, Jožef Stefan Institute, Jamova 39, 1000 Ljubljana, Slovenia

Abstract

In this study, nanocrystalline $LiFePO_4$/C composite powder has been synthesized via a cellulose matrix-assisted method. In an experiment conducted under extreme conditions involving rapid heating, short high-temperature delay, and subsequent quenching, well-ordered 35-nm crystallites have been obtained within five minutes. A quantitative filter paper has served both as a template and carbon source. It degrades pyrolytically through fragmentation reactions and formation of volatiles when exposed to rapid heating, which further has an impact on powder morphology, as revealed by electron microscopy studies. The electrochemical measurements in terms of galvanostatic

cycling have shown that the approach presented in this study may enable to reach good rate capability and excellent cycling stability.

Keywords: Lithium iron phosphate ($LiFePO_4$); Cathode materials; Rietveld X-ray refinement; Nanocrystalline materials; Cellulose template

Corresponding author: Dragana Jugović

Institute of Technical Sciences of SASA

Knez Mihailova 35/IV, 11 000 Belgrade, Serbia,

Phone: +381641177549,

Fax: +381112185263,

e-mail: dragana.jugovic@itn.sanu.ac.rs

1. Introduction

Olivine-type lithium iron phosphate is one of the most promising cathode materials for rechargeable batteries for large plug-in hybrid and all-electric vehicles of a great driving range [1]. Therefore, this material has been thoroughly studied during the past decade. The olivine structure typical of $LiFePO_4$ has a slightly distorted hexagonally-close-packed oxygen array. The divalent Fe^{2+} ions occupy corner-shared octahedra (denoted as M2 sites). The phosphorus ions are located in tetrahedral sites, and the lithium ions reside in chains of edge-shared octahedra (M1 sites) [2]. The structure may contain one lithium ion per formula unit, which results in the theoretical capacity of 170 $mAhg^{-1}$. Lithium motion within the olivine crystal structure occurs through one-dimensional (1D) channels

along the b axis [3]. These one-dimensional paths are particularly susceptible to blockage by defects and impurities [3, 4].

Numerous synthesis routes for obtaining both phase pure $LiFePO_4$ powders and $LiFePO_4$/carbon composites with good electrochemical performances have been explored so far [5]. During the synthesis procedure it is important to achieve the exact stoichiometry of cations in the precursor compounds, to mix them well, to increase the temperature, and to ensure an oxygen- and humidity-free environment in the high-temperature region. This namely means that a slightly reductive environment is preferred. Once this is ensured, phase pure $LiFePO_4$ will positively be obtained. However, having in mind the main drawbacks of this material, i.e. poor ionic and electronic conductivity, it is also important to ensure that the obtained particles be small and/or carbon-coated, or the particle morphology and texture be designed so as to obtain large surface areas. Coating with carbon is often performed by the *in situ* pyrolysis of an organic precursor, while different morphologies are obtained by combining soft chemical routes with conventional solid-state reactions [6]. Nanocasting of hard templates is also an effective method to obtain monolithic materials with largesurface areas and an open-porous structure. Both hard and soft templates, involving colloidal crystal [7], carbon monolith [8], and the combination of colloidal crystal templating with surfactant templating [9], glucose [10], triblockcopolymer [8, 11], and citric acid [6] have been employed to accommodate $LiFePO_4$ particles in porous carbon frameworks. Template approaches usually imply drawbacks such as high cost and complicated synthesis procedures that are difficult to transfer to large-scale commercial applications.

Bearing in mind that the simplicity of the synthesis process is vital for commercializing Li-ion batteries, we have developed a facile and fast templating, time- and energy saving method which employs commercial quantitative filter paper both as a template and carbon source. It does not involve any specific equipment, or expensive compounds, which is beneficial for commercial purposes. Furthermore, the whole procedure, from measuring the starting compounds to the final composite powder, is finished within an hour, making it competitive to other synthesis approaches. By rapid heating and a short delay at a high temperature with subsequent quenching, we attempted to control the crystal growth of initial crystallites and to preserve the well-ordered structure. Filter paper has already been used for the synthesis of another cathode material, $LiMn_2O_4$, as an exo-template that burns out on heating in air [12], but to the best of our knowledge, this has been the first attempt to use it as a template in the synthesis of $LiFePO_4$ under inert atmosphere. Quantitative filter paper is made of at least 98wt% of α-cellulose, which degrades pyrolytically through fragmentation reactions and the formation of combustible volatiles when exposed to rapid heating [13]. The temperature at which the pyrolysis of cellulose begins can be lowered by introducing some inorganic compound, when more char and noncombustible volatiles are produced. In this study, phosphoric acid in a precursor solution has also been used as a flame retardant [14].

2. Experimental

The precursor solution was prepared using water-based solution chemistry, and the precursors were chosen so as to prevent precipitation of the solution prior to infiltration.

The starting compounds were $LiNO_3$, $FeSO_4 \cdot 7H_2O$, and H_3PO_4 dissolved in water so as to keep the molar ratio of Li:Fe:P = 1:1:1. A quantitative filter paper (Sartorius, pore size 50 nm) was used as a template on which the precursor solution was instilled. The filter paper was first immersed into the precursor solution, and then squeezed between two glass sheets to remove bubbles and excessive liquid. This was done in order to achieve full control of the synthesis conditions, and to obtain good reproducibility. However, for the scale-up purposes the squeezing step can be skipped, by simply allowing excessive solution to decant from vertically positioned soaked paper. After that, the paper was left in air to dry and introduced into the furnace previously heated to 700 ºC for only 5 minutes, and subsequently quenched to room temperature. This was accomplished by means of a horizontal electric furnace equipped with a quartz glass tube with the opening on one side, while the flow of the reaction gas (Ar + 5% H_2) was enabled by a two-sided cap. The filter paper was placed in an alumina crucible inside the quartz glass tube. Although the olivine crystallization temperature is around 450 ºC [15], the chosen 700 ºC were expected to enable the *in situ* formation of conductive carbon [16].

X-ray powder diffraction data were collected on a Philips PW 1050 diffractometer with Cu-$K\alpha_{1,2}$ radiation (Ni filter) at room temperature. Measurements were done in a 2θ range of 10-110° with the scanning step width of 0.02° and 14-s intervals per step. The crystal structure refinement was based on the Rietveld full profile method [17] using the Koalariet computing program [18].

The thermal analysis of the sample was performed on a SDT 2960 simultaneous DSC–TGA TA Instruments in order to determine the carbon content [19].

The morphology of the synthesized powder was analyzed by scanning electron microscopy (TESCAN, MIRA3 XMU) at 20 kV and by transmission electron microscopy (JEOL JEM 2100) with an acceleration voltage of 200 keV.

Electrochemical measurements were carried out in a closed, argon filled two-electrode cell, with metallic lithium as a counter electrode. One-mole solution of $LiClO_4$ (p.a., Chemmetall GmbH) in PC (p.a., Honeywell) was used as electrolyte. The working electrode was made from the synthesized material, carbon black and polyvinylidene fluoride (PVdF, Aldrich) mixed in the 85:5:10 weight percent ratio and deposited on platinum foils from the slurry prepared in N-methyl-2-pyrrolidone. Galvanostatic charge/discharge tests were performed between 2.3 and 4.1 V at different current rates, using the Arbin BT 2042 battery test system. Since only $LiFePO_4$ within composite powder participates in the electrochemical reactions in the present voltage range, the mass of active material ($LiFePO_4$) was calculated by subtracting the mass of carbon from the whole mass of composite powder. Subsequently, the specific capacities were calculated using only the loading of active material on the electrode.

Results and Discussion

The morphology of the powder, as revealed by scanning electron microscopy, is shown in Fig. 1. The particles are irregular in shape and highly agglomerated, consisting of closely packed platelet-like structures giving rise to irregularly shaped pores of variable widths. Obviously, the products of cellulose pyrolysis, carbon and volatiles, had an impact on the powder morphology. However, this irregularity in shape is uniform for the whole sample;

accordingly it is impossible to differentiate between the two phases present in the composite powder by analyzing SEM images.

A more detailed analysis of particle microstructure was accomplished using high-resolution TEM images (Fig. 2). A HRTEM analysis revealed isles of crystalline $LiFePO_4$ domains within an amorphous carbon matrix. The electron diffraction ring pattern, to the right in Fig. 2, indicates the polycrystalline nature of the $LiFePO_4$ phase.

The crystal structure of the synthesized powder was confirmed by X-ray powder diffraction. The diffraction pattern revealed the $LiFePO_4$ phase of an olivine-type structure, with no impurity phases (Fig. 3). There is no evidence for the formation of crystalline carbon; therefore the internal amorphous nongraphitic carbon could be considered as a contribution to the background. The amount of the *in situ* formed carbon was determined thermogravimetrically and estimated at 40 wt%. The crystal structure refinement was based on the Rietveld full profile method [17] using the Koalariet computing program based on the Fundamental Parameters convolution approach to generate line profiles [18]. This program is suitable for processing data obtained from the samples with dominant microstructure parameters. The observed and calculated X-ray diffraction profiles of the sample are given in Fig. 3, while the main results of the final Rietveld refinement are presented in tables 1 and 2. The structure of the $LiFePO_4$ powder has been refined in the space group *P*nma (D_{2h}^{16}) in the olivine type with the following crystallographic positions: Li^+ ions in the special crystallographic position 4*a* [0,0,0] with local symmetry $\bar{1}$; Fe^{2+} and P^{5+} ions occupy two different crystallographic 4*c* positions [x,0.25,z] with the local symmetry m; O^{2-} ions occupy three different crystallographic positions: additional two 4*c* positions and one general 8*d* position [x,y,z] with the local

symmetry 1. The lattice parameters (Table 1) and the primitive cell volume (V= 290.6 $Å^3$) are slightly smaller than those reported in literature for stable and relaxed lattices found in single crystals (V=291.4 $Å^3$) [20] or powder annealed for a long period of time (36 h) at a sufficiently high temperature (V = 291.06 $Å^3$) [21]. Smaller values of lattice parameters may imply a vacancy in the structure. A small deviation of the oxygen site occupation factor from the unity indicates the presence of some oxygen vacancies restricted only to O1 and O3 oxygen crystallographic positions (the refined factors are 0.98 for both sites). Oxygen vacancy can appear as a result of additional reductive environment created by cellulose pyrolysis and/or by the quenching method. The Rietveld refinement has also shown an additional electron density on the lithium sites indicating the so-called "anti-site" defect in which a Li ion (on the M1 site) and an Fe ion (on the M2 site) are interchanged. This anti-site disorder (ca. 1-2 mol %) is believed to be an intrinsic property of the olivine $LiFePO_4$ [4]. There are several models that can describe the defect caused by the cation rearrangement: 1) an iron-rich model, $Li_{1-2y}Fe_yFePO_4$, and 2) a lithium–iron mixing model, $Li_{1-y}Fe_y[Li_yFe_{1-y}]PO_4$, with only Fe^{2+} ions taken into consideration, or 3) the existence of both cation vacancies and an anti-site disorder $({}_xLi_{1-x-y}Fe_y)({}_zFe_{1-z})PO_4$ with lithium deficiency and the presence of significant amounts of Fe^{3+}. However, from the Rietveld refinement of the X-ray diffraction data, we cannot distinguish between the formation of antisite defects and the usual lithium deficiency, due to the well-known small X-ray atomic scattering factor of lithium ions. The obtained values for microstrain and strain are refined to zero within an error tolerance, while the mean crystallite size is 35 nm.

Both refined and fixed fractional atomic coordinates (Table 2) were used to calculate all relevant bond distances and bond angles that enabled us to determine the coordination polyhedra. Some relevant bond distances are provided in Table 3. The calculated average Fe-O bond distance is larger, while the average P-O distance is smaller than those reported for single crystals [20], implying weakened Fe-O bonding and strengthened P-O bonding. Apparently, a change in electron distribution modifies the force constant of chemical bonds through an Fe-O-P inductive effect. A recent study perormed using *in situ* high-resolution electron microscopy [22] has demonstrated that in the case of lithium iron phosphate nanocrystals initial crystallites, formed after the nucleation during crystallization, have an ordered cation configuration, while in further crystal growth significant local cation disordering can be kinetically induced. Usually, further annealing of disordered crystallites provides sufficient time for atoms to arrange into a stable configuration in the lattice. However, such annealing and subsequent particle coarsening lead to increased crystallite sizes and sometimes to an additional cation disorder. Therefore, the control of crystal growth has great importance in maintaining the ordered arrangement between cations [22]. The synthesis method presented in this study – which involves rapid heating and cooling, together with short high-temperature delay – enabled us to control crystal growth and consequently resulted in small crystallites with a small amount of cation disordering and slight oxygen vacancies, as revealed by the XRD study. This was enabled by the *in situ* formation of carbon, which effectively impedes particle coarsening.

The electrochemical performances of the synthesized powder used as a cathode of a Li-ion battery were examined by charge-discharge tests. The galvanostatic cyclings

were done with the same current rate, for both charging and discharging processes. The discharge rates are given in C/n, where C is the nominal capacity equal to 170 mAh per gram of active material ($LiFePO_4$), and n is the discharge time given in hours needed for the complete discharge. Fig. 4 shows charge and discharge curves for the first 10 galvanostatic cycles. The specific capacity obtained at the 0.1 C current rate was 165 mAh per gram of active material $LiFePO_4$, that is 97% of the theoretical value for $LiFePO_4$, with a 100% charge/discharge efficiency. Apparently, a small amount of cation disordering did not block Li channels and hence full utilization of the material was achieved. The cycling performance at variable discharge rates is presented in Fig. 5. Evidently, the $LiFePO_4$/C electrode shows very good rate capability and excellent cycling stability. It is interesting to note that both charge and discharge curves (Fig. 4) have a profile somewhat different from that observed in most $LiFePO_4$ powders. Since both the removal and insertion of lithium ions are two-phased reactions, the characteristic feature of galvanostatic curves is a flat voltage plateau [23]. The sample under investigation shows an initial slope of the discharge curve, followed by a plateau, and then, towards the end of the discharge, another sloping region. In addition, a voltage plateau is not entirely flat but a little bit sloping, suggesting a compositionally narrower two-phase field. Having in mind the results of XRD and HRTEM studies, small crystallites of a vacant structure isolated and surrounded by conductive carbon, a possible explanation for the sloping voltage could be the decrease of the miscibility gap between the two end phases, $LiFePO_4$ and $FePO_4$. Namely, Yamada et al. [24] isolated solid-solution phases in Li_xFePO_4 at room temperature, suggesting an incomplete miscibility gap decreasing with decreased particle sizes. Furthermore Gibot et al. [25] reported that the inherent

crystalline disorder coupled with nano-crystallization below 40nm leads to a peculiar situation where the solid solution dominates most of the lithium compositional region in Li_xFePO_4, even at room temperature.

3. Conclusions

By conducting the experiment under extreme conditions involving rapid heating, short high-temperature delay, and subsequent quenching of filter paper soaked with the precursor solution, composite $LiFePO_4$/C powder has been obtained. The Rietveld refinement has confirmed that under such limited synthesis conditions ordered nanocrystallites were achieved. The electrochemical investigations have shown the full utilization of lithium iron phosphate in the composite powder at comparable small current rate (C/10), with excellent rate capability. Although high carbon yield in the composite powder is undesirable, this study offers a new insight into the crystal growth of $LiFePO_4$ and the possibility for its very fast synthesis.

Acknowledgements

The Ministry of Education, Science and Technological Development of the Republic of Serbia provided financial support for this study under grants nos. III 45004 and III 45015.

References

[1] J.B. Goodenough, Y. Kim, Chem. Mater. 22 (2010) 587.

[2] A. S. Andersson, B. Kalska, L. Häggström, J. O. Thomas, Solid State Ionics 130 (2000) 41.

[3] D. Morgan, A. Van der Ven, G. Ceder, Electrochem. Solid-State Lett. 7 (2004) A30.

[4] M. S. Islam, D. J. Driscoll, C. A. J. Fisher, P. R. Slater, Chem. Mater. 17 (2005) 5085.

[5] D. Jugović, D. Uskoković, J. Power Sources 190 (2009) 538.

[6] R. Dominko, M. Bele, J.-M. Goupil, M. Gaberscek, D. Hanzel, I. Arcon, J. Jamnik, Chem. Mater. 19 (2007) 2960.

[7] C. M. Doherty, R. A. Caruso, B. M. Smarsly, P. Adelhelm, C. J. Drummond, Chem. Mater. 21 (2009) 5300.

[8] C. M. Doherty, R. A. Caruso, B. M. Smarsly, C. J. Drummond, Chem. Mater. 21 (2009) 2895.

[9] A. Vu, A. Stein, Chem. Mater. 23 (2011) 3237.

[10] J. Zhao, J. He, J. Zhou, Y. Guo, T. Wang, S. Wu, X. Ding, R. Huang, H. Xue, J. Phys. Chem. C 115 (2011) 2888.

[11] X. L. Wu, L. Y. Jiang, F. F. Cao, Y. G. Guo, L. J. Wan, Adv. Mater. 21 (2009) 2710.

[12] M. W. Raja, S. Mahanty, R. N. Basu, J. Mater. Chem. 19 (2009) 6161.

[13] M. J. Jr. Antal, G. Varhegyi, Ind. Eng. Chem. Res. 34 (1995) 703.

[14] K.C. Patil, J.P. Vittal, C.C. Patel, Thermochimica Acta 43 (1981) 213.

[15] J. Moskon, R. Dominko, M. Gaberscek, R. Cerc-Korosec, J. Jamnik, J. Electrochem. Soc. 153 (2006) A1805.

[16] M. Doeff, Y. Hu, F. McLarnon, R. Kostecki, Electrochem. and Solid State Lett. 6 (2003) A207.

[17] H.M. Rietveld, J. Appl. Cryst. 2 (1969) 65.

[18] R.W. Cheary, A. Coelho, J. Appl. Cryst. 25 (1992) 109.

[19] Sh. Yang, Y. Song, P. Y. Zavalij, M. S. Whittingham, Electrochem. Commun. 4 (2002) 239.

[20] V. A. Streltsov, E. L. Belokoneva, V. G. Tsirelson, N. K. Hansen, Acta Cryst. B 49 (1993) 147.

[21] A. S. Andersson, B. Kalska, L. Häggström, J. O. Thomas, Solid State Ionics 130 (2000) 41.

[22] S.-Y. Chung, Y.-M. Kim, S. Lee, S. H. Oh, J.-G. Kim, S.-Y. Choi, Y.-J. Kim, S.-J. Kang, Nano Lett. 12 (2012) 3068.

[23] J. Chen, M. J. Vacchio, S. Wang, N. Chernova, P. Y. Zavalij, M. S. Whittingham, Solid State Ionics 178 (2008) 1676.

[24] G. Kobayashi, S. Nishimura, M.-S. Park, R. Kanno. M. Yashima, T. Ida, A. Yamada, Adv. Funct. Mater. 19 (2009) 395.

[25] P. Gibot, M. Casas-Cabanas, L. Laffont, S. Levasseur, P. Carlach, S. Hamelet, J.-M. Tarascon, C. Masquelier, Nat. Mater. 7 (2008) 741.

Table 1. The final results of the Rietveld structural refinement.

Lattice parameters (Å)	a = 10.3131(9) b = 6.0025(8) c = 4.6948(6)
Primitive cell volume ($Å^3$)	290.6(1)
Mean crystallite size (nm)	35(2)
Li site occ. by Fe	0.024(9)
R_B factor (%)	2.20

Table 2. Fixed and refined atomic coordinates and isotropic displacement parameters.

fractional coordinates	x	y	z	B ($Å^2$)
Li (4*a*)	0	0	0	3(1)
Fe (4*c*)	0.2815(3)	0.25	0.9780(12)	1.4(2)
P (4*c*)	0.0964(8)	0.25	0.4156(19)	0.5(2)
O(1) (4c)	0.098(2)	0.25	0.734(3)	1.1(3)
O(2) (4c)	0.457(2)	0.25	0.212(2)	1.1(3)
O(3) (8d)	0.162(1)	0.050(2)	0.281(1)	1.1(3)

Table 3. Selected bond lengths (in Å) for $LiFePO_4$.

Fe – O(1)	2.2098
Fe – O(2)	2.1126
Fe – O(3) x 2	2.2310
Fe – O(3)' x 2	2.1086
$(Fe – O)_{aver.}$	2.1669
Li – O(1) x 2	2.2011
Li – O(2) x 2	2.0701
Li – O(3) x 2	2.1486
$(Li – O)_{aver.}$	2.1399
P – O(1)	1.4935
P – O(2)	1.5603
P – O(3) x 2	1.5153
$(P – O)_{aver.}$	1.5211

Figure captions

Fig. 1. SEM micrograph of the synthesized powder.

Fig. 2. HRTEM image and electron diffraction pattern of the synthesized powder.

Fig. 3. The observed (•), calculated (-), and the difference between the observed and calculated (bottom) X-ray diffraction data taken at room temperature. Vertical markers bellow the diffraction patterns indicate positions of possible Bragg reflections for olivine type $LiFePO_4$.

Fig. 4. Galvanostatic charge-discharge curves of the synthesized powder at 0.1 C rate.

Fig. 5. The cycling performance and charge-discharge curves at different current rates (inset).

Figure 1

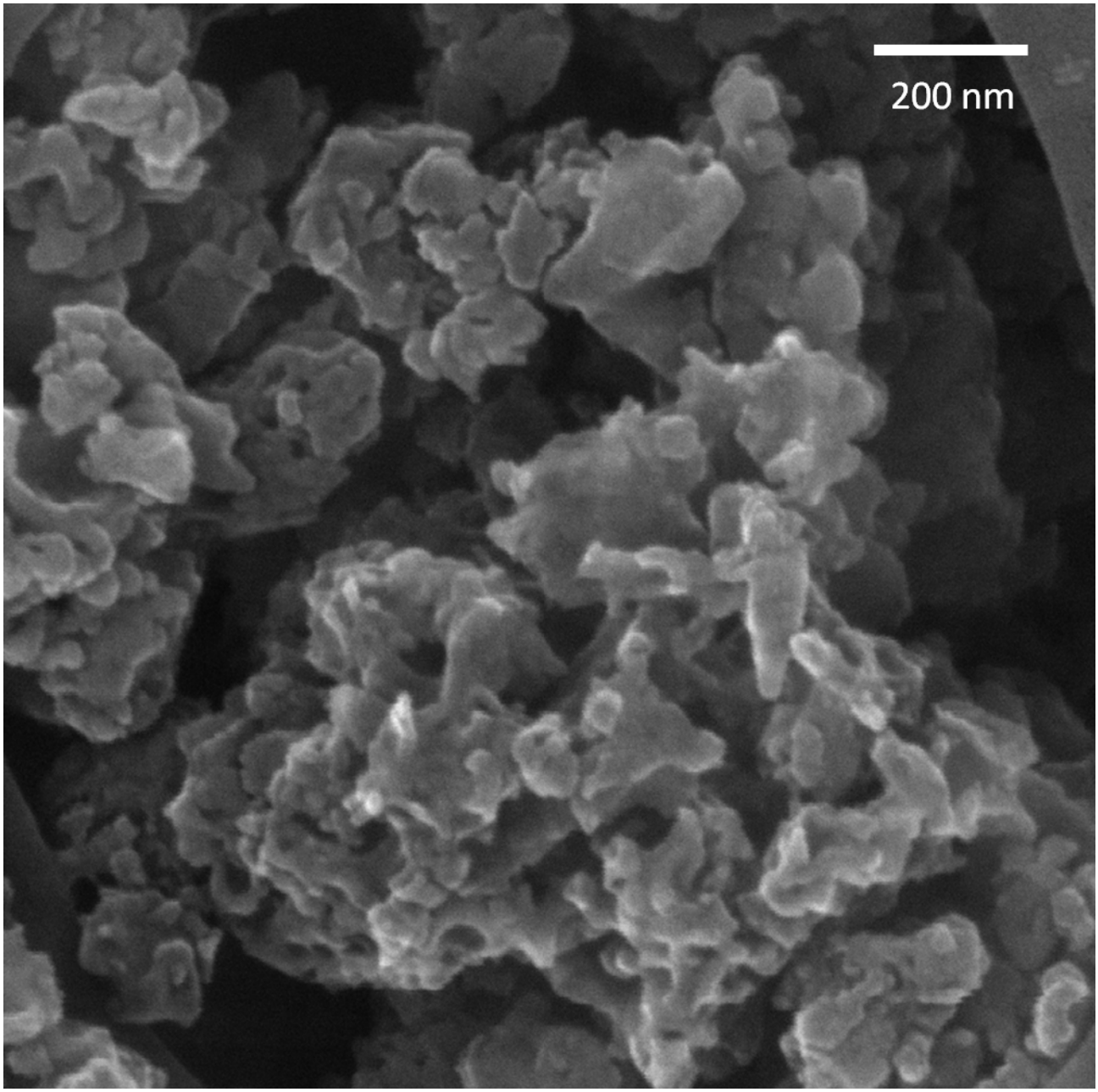

Figure 2

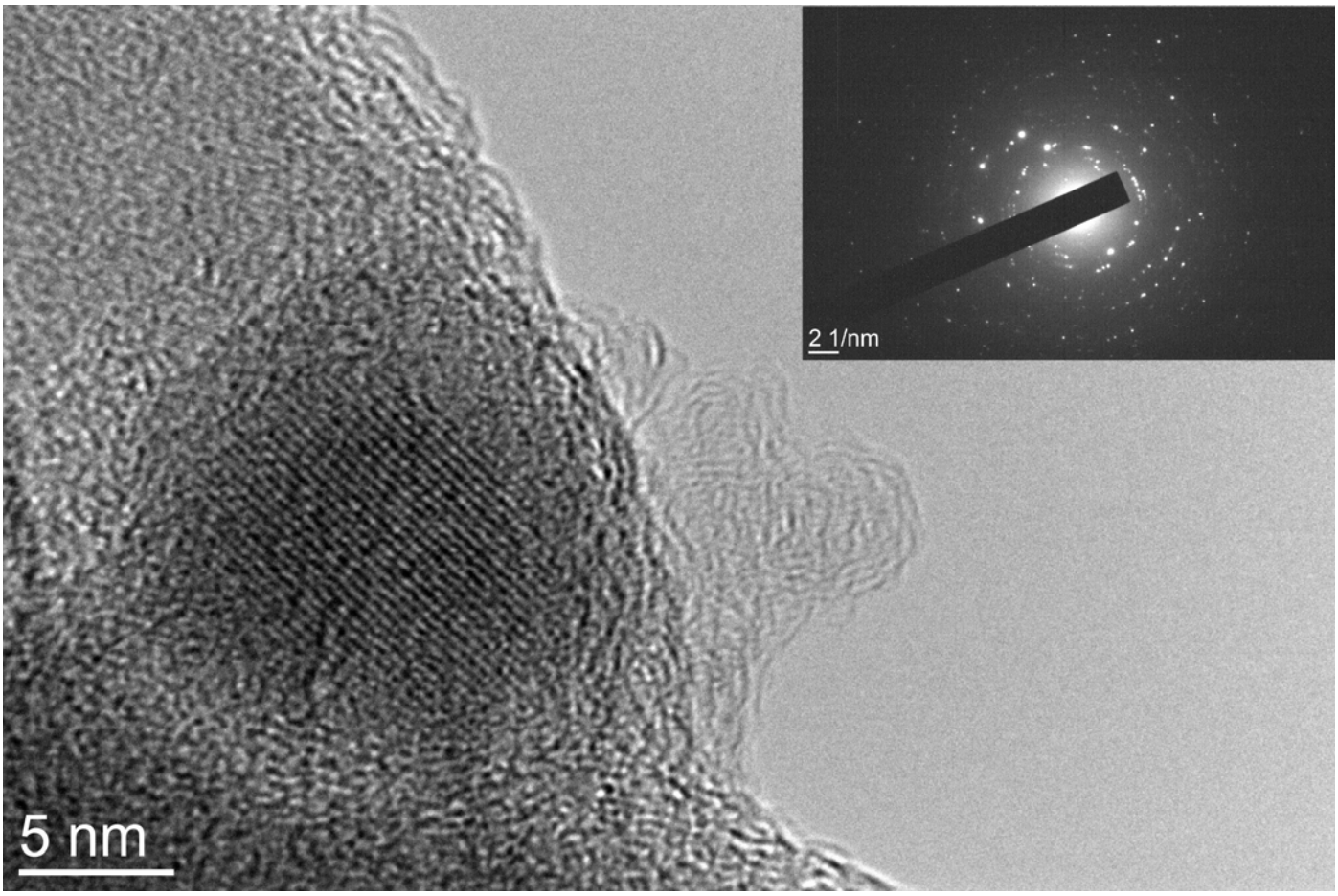

Figure 3

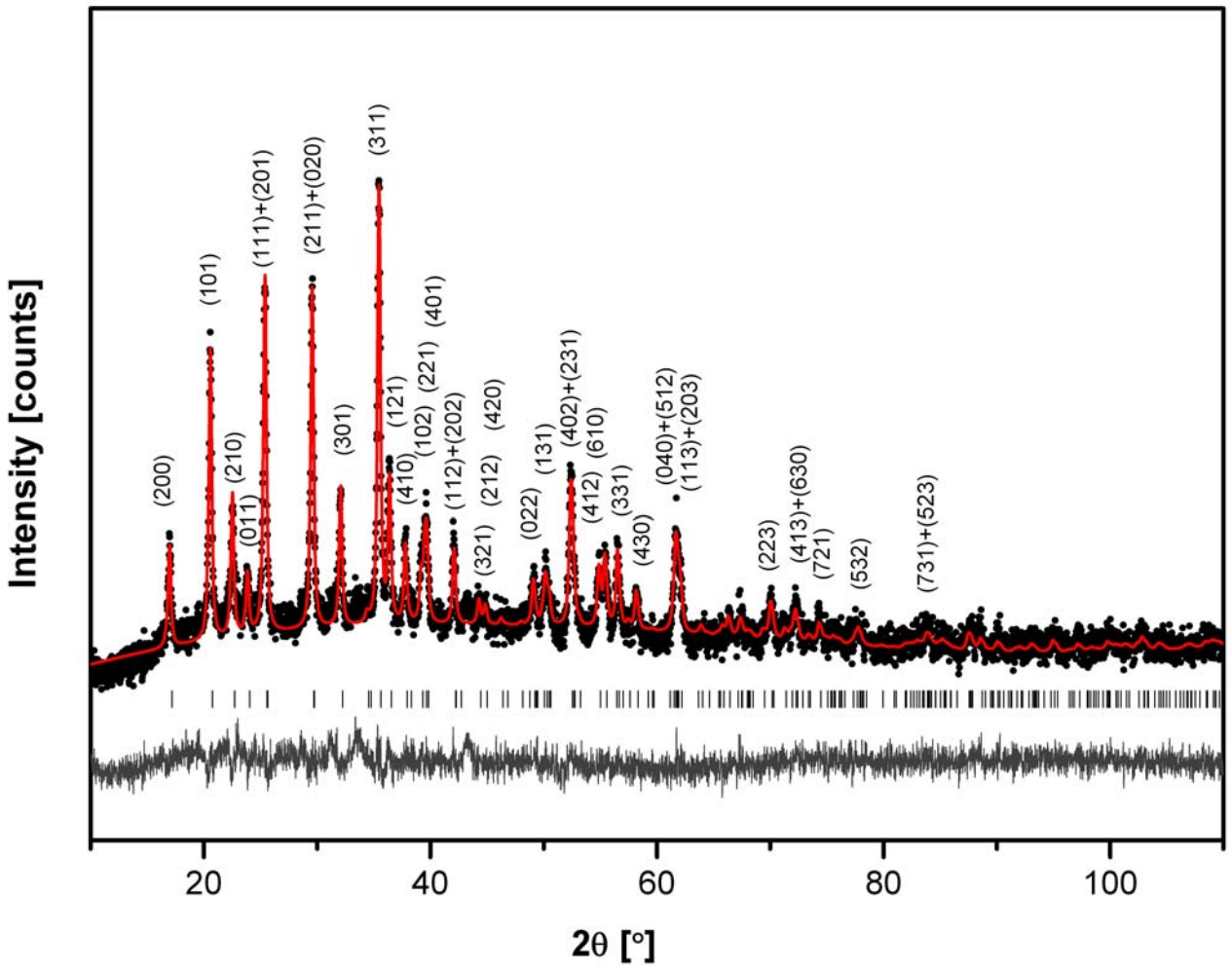
Intensity [counts]
(200)
(101)
(210)
(011)
(111)+(201)
(211)+(020)
(301)
(311)
(121)
(410)
(102)
(221)
(401)
(112)+(202)
(321)
(212)
(420)
(022)
(131)
(402)+(231)
(412)
(610)
(331)
(430)
(040)+(512)
(113)+(203)
(223)
(413)+(630)
(721)
(532)
(731)+(523)
20
40
60
80
100
2θ [°]

Figure 4

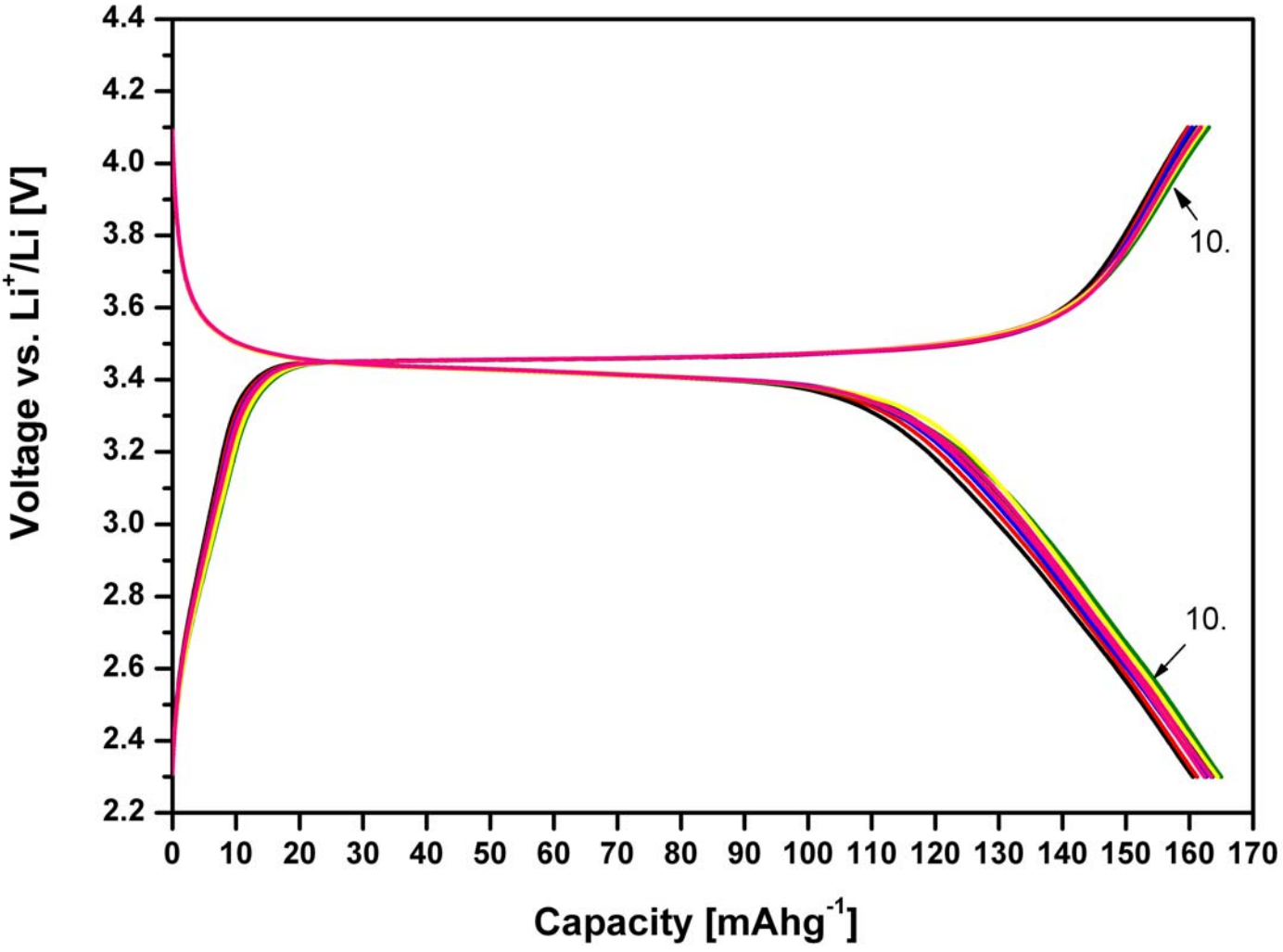
Voltage vs. Li+/Li [V]
4.4
4.2
4.0
3.8
3.6
3.4
3.2
3.0
2.8
2.6
2.4
2.2
0
10
20
30
40
50
60
70
80
90
100
110
120
130
140
150
160
170
Capacity [mAhg-1]
10.
10.

Figure 5

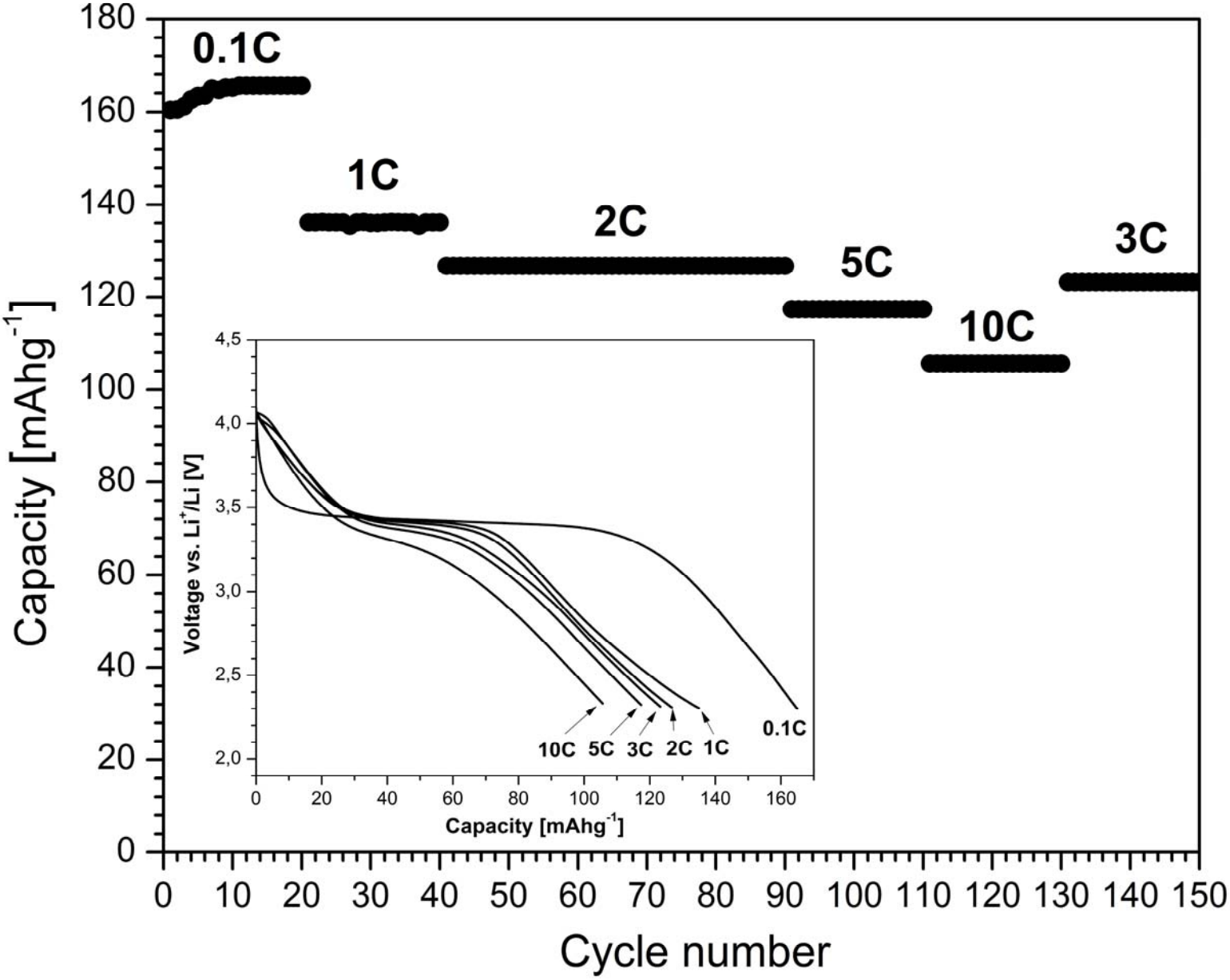
0.1C
1C
2C
5C
10C
3C
Capacity [mAhg-1]
Cycle number
Voltage vs. Li+/Li [V]
Capacity [mAhg-1]
10C
5C
3C
2C
1C
0.1C